JOURNAL OF MATERIALS SCIENCE **40** (2005) 3503–3508

Effects of self-affine surface roughness on the adhesion of metal-polymer interfaces

R. VAN TIJUM, J. TH. M. DE HOSSON*
Department of Applied Physics, Materials Science Centre and the Netherlands, Institute for Metals Research, University of Groningen, Nijenborgh 4, 9747 AG Groningen, The Netherlands
E-mail: j.t.m.de.hosson@rug.nl

This paper concentrates on a theoretical examination of the influence of roughness on the adhesive properties along metal-polymer interfaces. An algorithm has been designed to generate a self-affine surface roughness. It has been used to examine influence of the Hurst exponent on the interface strength during a pull-off test of metal-polymer laminates. The generated surfaces are implemented in a cohesive zone model representing the interface between a coated steel and polyethylene terephthalate (PET). From the model it can be concluded that a small increase in surface area is linear with the interface strength. This relation does not hold when the increase in surface area becomes larger than 150%. The deviation from the linear relationship increases with smaller Young's moduli. This is caused by the reduced elastic energy storage in the polymer when local surface characteristics become more important.

1. Introduction

Metal-polymer laminates are used in daily products, in particular in food industry such as in cans. For the production of these laminates several methods exist to adhere the polymer film to the metal. The strength of the interface between the metal and the steel depends on various aspects, one of which is the surface morphology of the metal. Already in the early eighties of the last century it was recognized that surfaces can be described by self-affine fluctuations [1] and surfaces of rolled metal appeared to be also self-affine rough. The effect of the self-affine roughness on the interface strength is addressed in this paper from a numerical viewpoint. To determine the influence of the surface roughness on the interface strength a finite element model is presented in which a cohesive zone defines the interface between the polymer and the metal.

Surfaces for the cohesive zone model were created with a modified version of the so-called Voss [2] algorithm. The Voss algorithm is based on the assumption that there is no preconditioned correlation length. In this algorithm, points which are located a distinct distance apart, are given randomly varying Gaussian amplitude (w). The points that have been moved are connected with straight lines. The rest of the points are placed along these lines (Fig. 1). At each refinement step the distance is divided by 2 and the amplitude of the normal distributed Gaussian noise is reduced according to the following equation:

$$w_i = w_{\text{initial}}\lambda^{2\alpha i} \quad \text{with } i = 1, 2, \ldots, ^2\log(N-1) \quad (1)$$

In Equation 1 i is the refinement step number, α the Hurst exponent, λ the lacunarity (normally 0.5), w_{initial} the initial roughness amplitude and N is the total number of points of the final surface. This algorithm is also tractable in more dimensions, but for the sake of simplicity in the rest of the paper 1D has been assumed.

Unfortunately the Voss algorithm as such is not able to generate surfaces with specific topological properties. In fact we are interested in an algorithm, which is able to generate surfaces as a function of the number of surface points (N), RMS roughness amplitude (w), correlation length (ξ) and Hurst exponent (α). In order to generate these surfaces, we have chosen to adjust the amplitude (w_i) of each refining step in such a way that the generated random rough surface obeys predefined parameters. An easy way to express these values is using a height-height correlation:

$$H(r) = \frac{1}{N-r}\sum_{i=1}^{N-r}(h(r) - h(r+i))^2 \quad (2)$$

while self-affine surfaces can be described as [3]:

$$H(\rho) = 2w^2\left(1 - e^{-\left(\frac{\rho}{\xi}\right)^{2\alpha}}\right) \quad \text{with } 0 < \alpha < 1 \quad (3)$$

In fact Equations 2 and 3 are equal to each other except that Equation 3 describes a continuous ($H(\rho)$) and Equation 2 the discrete height-height correlation ($H(r)$). Because the final surface height-height correlation is known (Equation 3), it is important to know

*Author to whom all correspondence should be addressed.

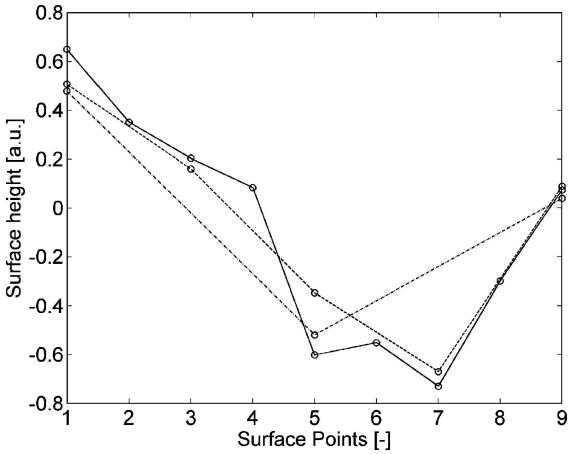

Figure 1 Refinement algorithm used by R.F. Voss ($N = 9$, $w_{\text{initial}} = 1$, $r = 0.5$, $\alpha = 0.5$): .- first step; --second step; - final surface.

how each refinement step contributes to the final surface ($h(r)$). It is straightforward to see that the addition of two fully Gaussian random surfaces has a height-height correlation that is equal to the addition of both height-height correlations. If the number of surface points is not infinite the total height-height correlation for all the Voss additions becomes:

$$H(r) = \sum_{i=1}^{^2\log(N-1)} H_i(r) \tag{4}$$

In Fig. 2 the height-height correlation functions of each refinement step is shown. In this figure only the number of surface points and the refinement step determines the shape of the curves. For all these curves the initial standard deviation (w_i) is set to equal to unity. The summation of all these curves (Equation 4) will produce a height-height correlation function that depends on the amplitude of each curve. By exactly describing the height-height correlation function for each step, the problem of generating self-affine surfaces becomes a problem of finding the right amplitude of each refinement step. Nonetheless, for the description of the height-height correlation function of a single refinement step we need to describe all the properties of this step and by combining these properties we should be able to describe the whole curve.

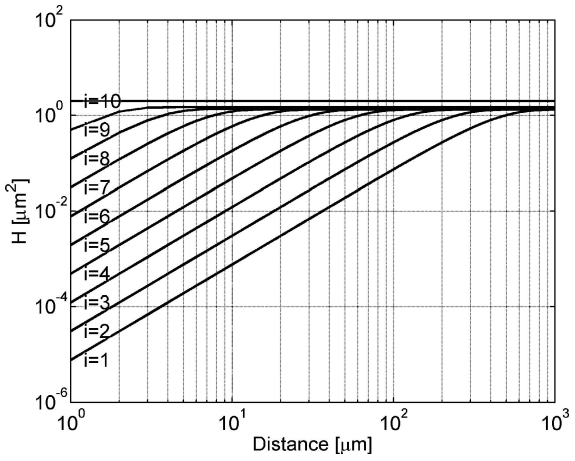

Figure 2 Contribution of each Voss refinement step for a surface with 1025 points and initial rms roughness $w_i = 1$ according to Equation 9.

The height-squared-difference of two neighboring points is:

$$H_i(1) = \frac{2w_i^2}{d_i^2} = \frac{2^{2i+1}w_i^2}{(N-1)^2} \tag{5}$$

with the distance between two displaced points equal to $d_i = \frac{N-1}{2^i}$.

Because of extrapolation, the actual standard deviation ($\sigma_{i,\text{actual}}$) will be lower than the initial standard deviation (Fig. 2) and this affects Equation 3. For a fully Gaussian surface the Hurst exponent α equal is to 1 and the lateral correlation length becomes:

$$\xi_i = \frac{1}{\sqrt{-\log\left(1 - \frac{w_i^2}{d_i^2\sigma_{\text{i,actual}}^2}\right)}} = \frac{1}{\sqrt{-\log\left(1 - \frac{4^i w_i^2}{(N-1)^2\sigma_{\text{i,actual}}^2}\right)}} \tag{6}$$

The ratio between the initial standard deviation (w_i) and the actual standard deviation ($\sigma_{\text{i,actual}}$) can be written as a function of the refinement step (i) and the surface size (N):

$$\frac{\sigma_{i,\text{actual}}^2}{w_i^2} = \frac{1}{d_i}\sum_{j=1}^{\text{distance}_i}\left(1 - \frac{j}{d_i}\right)^2 + \left(\frac{j}{d_i}\right)^2 = \frac{1}{3}\left(2 + \frac{4^i}{(N-1)^2}\right) \tag{7}$$

Taking Equations 3, 6 and 7 the height-height correlation function of one added Voss surface can be described by only three parameters: rms surface roughness (w_i) surface size (N) and refinement step (i) according to:

$$H_i(r) = 2\sigma_{i,\text{actual}}^2\left(1 - e^{-\left(\frac{r}{\xi_i}\right)^2}\right) = \frac{2}{3}\left(2 + \frac{4^i}{(N-1)^2}\right) \times \left(1 - \left(\frac{6(N-1)^2}{4^i + 2(N-1)^2} - 2\right)^{r^2}\right)w_i^2 \tag{8}$$

By calculating the height-height correlation for several distances (r), it is possible to generate a set of linear equations having the form:

$$2 \cdot A \cdot (w^2) = H(r) \tag{9}$$

In Equation 9 the expected height-height correlation ($H(r)$) is defined by Equation 3 and the square matrix (A) is then defined by:

$$A(r,i) = \frac{1}{3}\left(2 + \frac{4^i}{(N-1)^2}\right) \times \left(1 - \left(\frac{6(N-1)^2}{4^i + 2(N-1)^2} - 2\right)^{r^2}\right) \tag{10}$$

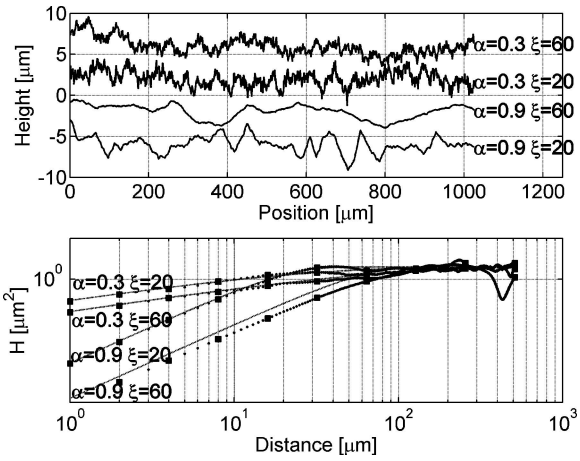

Figure 3 Generated surface profiles (top) and height-height correlations (bottom): .. requested height–height correlation; ■ samplepoint; ● calculated height–height correlation.

According to Equations 9 and 10 it is important to choose the distances (r) with care. The height-height correlation function is an exponential function and the distance between two points is also a power of the refinement step. Both arguments yield to the same choice or the distances (r):

$$r_j = 2^j - 1 \quad \text{with } j = 1, 2, \ldots, {}^2\log(N-1) \quad (11)$$

The refinement step (i) will cover the same values as j. Combination of Equation 10 with Equation 11 generates the square matrix (A) for a given number of surface points (N). If the square matrix (A) is non-singular, there is a unique solution of Equation 9. This solution could contain negative values ($w_i^2 < 0$), which will cause an imaginary surface. The only way to tackle this problem is to find a solution that is very close to Equation 9 with non-negative w_i^2. For this problem several solvers are available in literature [4–6]. Now, the coefficients (w_i) for the Voss algorithm. Can be found by solving Equation 9 for a given number of surface points, correlation length, Hurst Exponent and RMS roughness amplitude. Some examples of a generated surface are shown in Fig. 3.

2. Results

The algorithm as described is used to generate a self-affine rough interfaces. These interfaces are implemented as a cohesive zone [7] in a finite element model [8]. The cohesive zone model was chosen, because substantial changes in height will cause preferably shear deformation and fracture instead of normal fracture. The geometry of the model we used is axis-symmetric (Fig. 4) with respect to the z-axis, which is also the pulling direction. The thickness of the polymer layer is 40 μm. Two cylindrical metal plates with a thickness of 20 μm and radius 2049 μm encloses the polymer. Because of symmetry only half of this system is modeled. The cohesive zone is laid in between the metal and the polymer. The polymeric and metal descriptions are based on quadrilaterals. In the model the size of these cells is set to 1×1 μm.

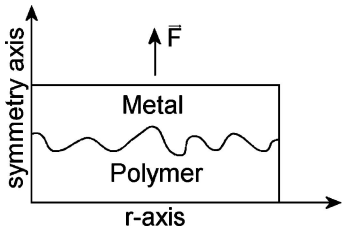

Figure 4 Schematic picture of the model.

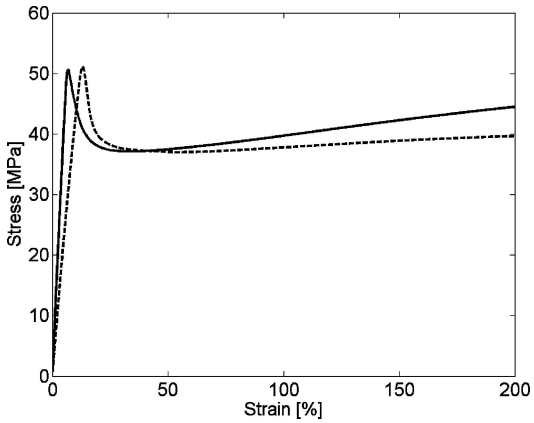

Figure 5 Calculated stress-strain response of PET (-) and the hypothetical polymer (--).

As a material system a chromium-plated steel with a polyethylene terephthalate (PET) coating was chosen. The response stress-strain response of the model [8] was fitted to the properties of PET [9] and the modeled stress-strain behavior of the polymer is displayed in Fig. 5. Further a hypothetical polymer is shown with approximately the same properties except that it has one half the Young's modulus of PET.

For the determination of the shear and normal response of the cohesive zone various peel-tests were performed. For this test we used a tensile stage inside an environmental scanning electron microscope (Philips-XL30-FEG ESEM) to prevent charging of the deformed polymer. From the scanning electron microscope observations, i.e. from both plane and cross-sectional view (Fig. 6) we were able to estimate the angle between

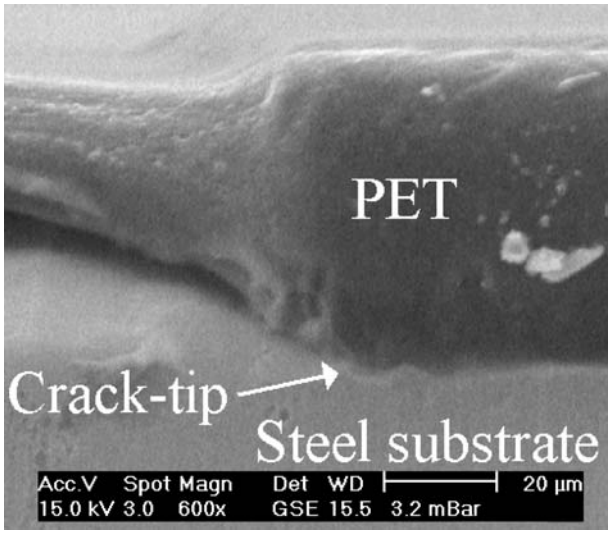

Figure 6 Environmental scanning electron microscopy observations during a zero degrees peel-test.

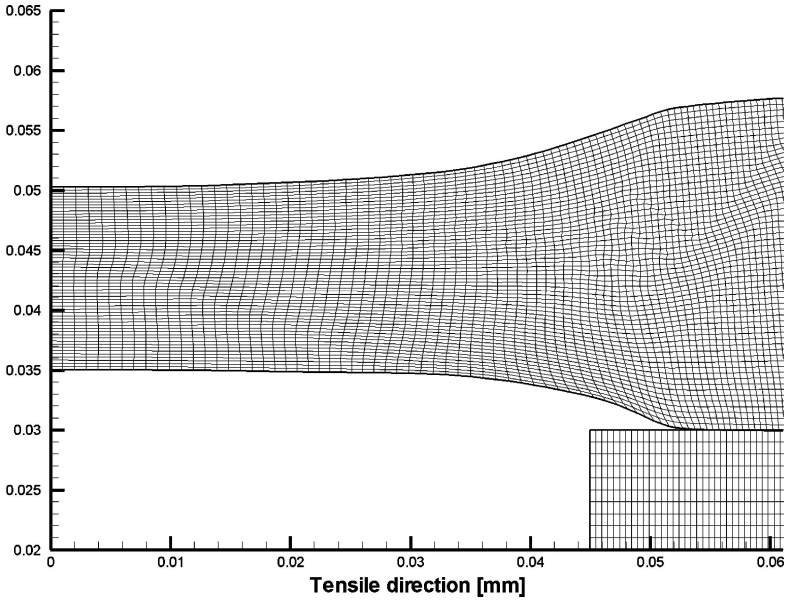

Figure 7 Simulation of a 30 μm thick coating during a 0 degrees peel-test.

the applied displacement of 0 degrees and the approximate 20 degrees at the crack-tip. The peel-tests were performed under 0 degrees, i.e. fully under shear. Because of the necking of the polymer the crack-tip was around 20 degrees instead of the global 0 degrees. In addition pull-off tests were performed to measure the maximum stress at normal opening for layer thickness of approximate 50 μm between 2 rigid steel plates. By performing several plane-strain simulations (Fig. 7) with different shear to normal ratios we were able to reach good agreement with the experiments. The cohesive zone employed is shown in Fig. 8. The graph explains the relationship between the normal and the shear traction. In the beginning of an experiment the cohesive zone has a zero thickness. Due to loading the traction-separation law will result in opening or shearing. When large shear traction is applied, the maximum normal traction is reduced and vice versa. It is important to emphasize that normal and shear traction are coupled.

During an experimental pull-off test the loading curve will increase until fracture occurs. At that point

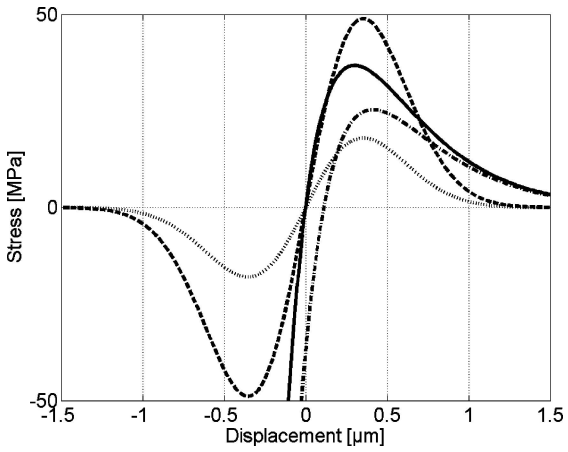

Figure 8 Response of the cohesive zone: - normal traction; -- shear traction; .- normal traction at maximum shear stress; .. shear traction at maximum normal stress.

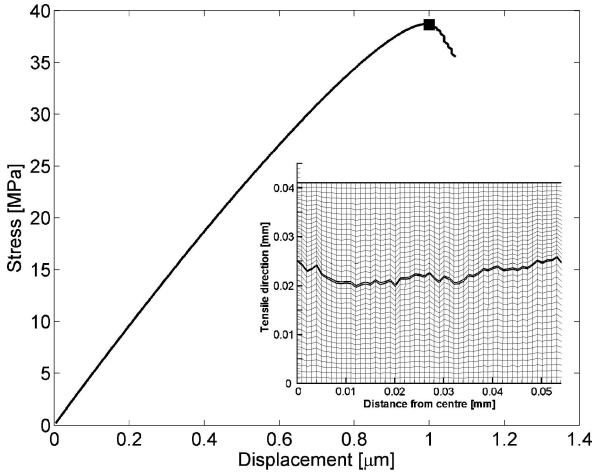

Figure 9 Stress displacement curve for $w = 3$; $\xi = 29$ and $\alpha = 0.6$. The square denotes at which stress the deformed mesh in the inset is taken.

the loading curve drops asymptotically towards zero. In the model description this instability also occurs. In Fig. 9 a typical curve is shown together with the deformed mesh at maximum stress. During the displacement controlled test the cohesive zone elements starts to fracture (the stress in the cohesive zone element has passed the maximum value). Less cohesive zone elements have to cope with the still increasing global stress, which results in an increase in fractured elements. This exponential behavior causes the finite element model to fail. According to Fig. 8 cohesive zone elements still function under compression or after reaching a certain maximum stress level, making this cohesive zone able to work without interference up to the instability point. However, to avoid this instability we will concentrate only on the maximum stress of the force displacement curve.

We have calculated three different Hurst exponents (0.3, 0.6 and 0.9) and rms roughness of 3 μm. A large Hurst exponent means that the surface is locally flat. Smaller values stand for large deviations from flatness

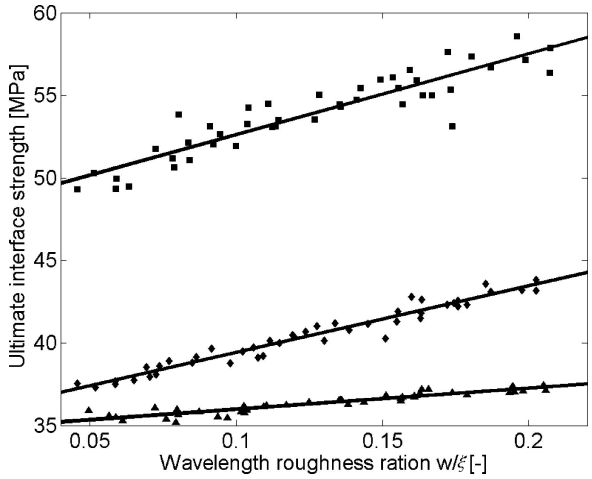

Figure 10 Maximum stress as a function of the ratio w/ξ: ■ $\alpha = 0.3 \pm 5\%$; ♦ $\alpha = 0.6 \pm 5\%$; ▲ $\alpha = 0.9 \pm 5\%$.

at shorter distances. For each Hurst exponent various surfaces with different lateral correlation lengths are calculated. These surfaces were used in the model calculations of the maximum stress. Fig. 10 shows that the lower Hurst exponents achieve a larger maximum stress level before failure. Obviously this is caused by the larger surface, which is inevitably with a jittery surface. The increase in surface area involves a larger angle between the normal and the shear stress at the interface (Fig. 11). This angle was calculated by averaging the angle of shear and normal stress over the whole surface at the maximum global stress level. During a pull-off test a large value of this angle already emerges at the beginning of a test. This emphasizes the fact that for large roughness a cohesive zone also needs to incorporate shear stresses.

The maximum stress level can also be presented as a function of the relative area. As indicated in Fig. 12 an increase of the surface area causes an increase of the maximum stress level. In the case of a small increase of the surface area the maximum stress level is linear with the increase in area. The relation holds up to relatively larger areas but eventually deviation from linearity occurs. In Fig. 12 also the results for a hypothetical polymer is implemented which has one half the

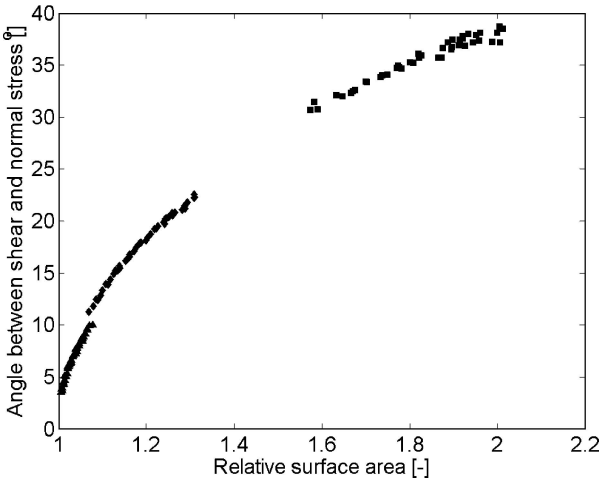

Figure 11 Average angle between shear and normal stress: ■ $\alpha = 0.3 \pm 5\%$; ♦ $\alpha = 0.6 \pm 5\%$; ▲ $\alpha = 0.9 \pm 5\%$.

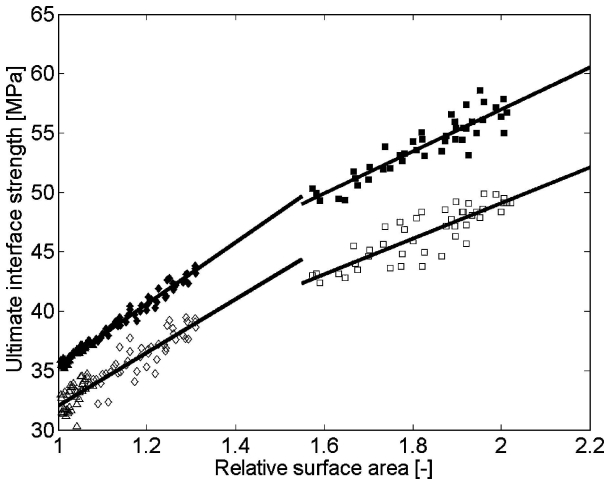

Figure 12 Maximum stress as a function of the relative area for PET (filled symbols) and the hypothetical polymer (open symbols): ■ $\alpha = 0.3 \pm 5\%$; ♦ $\alpha = 0.6 \pm 5\%$; ▲ $\alpha = 0.9 \pm 5\%$.

Young's modulus of polyethylene terephthalate (PET) keeping the other properties constant. Because of the smaller Young's modulus the elastic energy storage is reduced and a lower failure stress is found. For both cases the response of the increase of the relative surface area is similar. It is important to note the doubled deviation effect for the hypothetical polymer.

3. Discussion and conclusions

A self-affine roughness model is designed which can generate reproducible random rough surfaces. The model can be easily extended to a 3D description. A problem is that in some cases there is not a unique solution of Equation 9. The positive point is that the set of linear equations obtained is quite limited in size, only depending on the number of points in one direction, and making the algorithm useful for solving a 3D problem. The algorithm described can generate a set of self-affine rough surface points. The number of points is fixed after generating the surface. This is in contrast with existing theoretical approaches [2].

Thin adhesive layers already proved to be stronger than the material it is made of. This behavior is confirmed in the Figs 10 and 12. In the latter a large maximum stress distribution for rougher surfaces can be seen. This broad distribution is the result of the limited number of points used in the cohesive zone model. For the hypothetical polymer with half the Young's modulus of PET this distribution is even larger. This is mainly caused by the lower energy elastic storage that incorporates larger deformations. In that case local surface characteristics start to play an important role by generating locally voids. These local effects influence the maximum stress level to a large extent.

It is important to note that the surfaces used in the model calculations are assumed to be fully covered with the polymer. This is not always correct [10] and partial wetting may lead to partial detachments. In practice wetting could give problems on these very rough surfaces but it will strengthen the effects of roughness. Another minor problem could be that loose cohesive zone elements start to penetrate other cells. Within the

numerical experiments presented here this event did not occur.

The model described uses both normal and shear components to prove that increase of surface area does not linearly depend on the interface strength. For larger Hurst exponents the surface area increase is small. In that case the surface area and maximum stress have a linear relationship. When the surface becomes rougher, the mean angle between the tensile direction and the surface becomes so high that shear starts to play a role. As a consequence the linear relationship does not hold for small Hurst exponents or very small lateral correlation lengths. Local interface effects start to play an important role. This is also the cause of the larger deviations of the maximum stress. These local effects increase for polymers with lower Young's moduli strengthened by the reduced elastic storage.

Acknowledgements

This work was financially supported by the Netherlands Technology Foundation STW (project number GTF.4901).

References

1. B. MANDELBROT, "The Fractal Geometry of Nature" (Freeman, New York, 1977).
2. R. F. VOSS, "Random Fractal Forgeries," in Fundamental Algorithms in Computer Graphics, edited by R. A. Earnshaw (Springer-Verlag, Berlin, 1985) p. 805.
3. S. K. SINHA, E. B. SIROTA, S. GAROFF and H. B. STANLEY, *Phys. Rev. B* **38** (1988) 2297.
4. J. MORÉ, B. GARBOW and K. HILLSTROM, User Guide for MINPACK-1, Argonne Nat. Lab. Rep. ANL-80-74, 1980.
5. Optimalization Toolbox, The MathWorks Inc., 2001.
6. K. E. ATKINSON, "An Introduction to Numerical Analysis", 2nd ed. (John Wiley and Sons, 1988).
7. X.-P. XU and A. NEEDLEMAN, *Model. Simul. Mater. Sci. Eng.* **1** (1993) 111.
8. ABUL-BAQI, Failure of Brittle Coatings on Ductile Metallic Substrates, Shaker Publishing, 2002. Mech., A/Solids 16, special issue, (1997) 87.
9. W. P. VELLINGA, R. RASTOGI and H. E. H. MEIJER, *Mat. Res. Soc. Sym. Proc.* **695** (2002).
10. G. PALASANTZAS and J. TH. M. DE HOSSON, *Phys. Rev. E* **67** (2003) 021604.

Received 20 August 2004
and accepted 1 February 2005